Mechanism of spin-dependent inelastic scattering in the $^{13}C+^{12}C$ system

D. P. Bybell,* W. K. Wells,† and D. P. Balamuth
Department of Physics, University of Pennsylvania, Philadelphia, Pennsylvania 19104
(Received 19 February 1985)

The spin-flip probability has been measured using the Schmidt particle-γ coincidence technique for the reaction $^{12}C+^{13}C\rightarrow^{12}C^*+^{13}C$ leading to the first excited state of ^{12}C at energies $E_{c.m.}=17.28$ and 26.88 MeV. Both forward and backward angles in the center of mass system were studied, the latter only at the lower bombarding energy. The particle-γ angular correlation has also been measured in the reaction plane. The data have been analyzed by treating the elements of the density matrix of the final 2^+ state as unknown parameters using a least squares fitting procedure. The results of this analysis have been compared with reaction model calculations, and suggest that the observed spin-flip probability can be accounted for without the necessity of introducing a phenomenological spin-dependent component into the nucleus-nucleus optical potential.

I. INTRODUCTION

The question of the origin of spin-dependent effects in the scattering of composite objects such as light nuclei has stimulated considerable recent effort, both theoretical and experimental.[1–12] Experimentally, measurements have been made of a number of spin-dependent observables in the elastic and inelastic scattering of light heavy ions. The Heidelberg data[1] involving the scattering of polarized ^{6}Li and ^{7}Li nuclei from a variety of targets are by now well known. For heavier projectiles, the most recent work has involved studies of the spin orientation of a reaction product by coincident observation of a subsequent decay. The most frequently used technique at low energies is probably the Schmidt method[13] for inelastic scattering; two recent papers[2,5] have described observations of a nonzero spin flip following inelastic scattering in this way. At higher energies a variety of experimental techniques have been used, including measuring the polarization of reaction products using the β-asymmetry[8] or γ-ray circular polarization,[9] among others. (A recent review of experiments in the energy regime appropriate to deep inelastic scattering has been given by Dünnweber.[10]) Also, indirect evidence for what appear to be spin dependent effects has been inferred from a careful study of the angular distributions in single nucleon transfer reactions to final states with selected quantum numbers, usually two members of a spin-orbit doublet.[3,4] The analysis of these measurements is not model independent, however, and alternative explanations for the observed effects have recently been proposed.[11]

On the theoretical side, two basic approaches to the problem have been explored. The first of these consists in using the folding model to calculate the interaction between the nuclei in terms of an assumed density distribution and nucleon-nucleon interaction. It is assumed that the constituent nucleons are "frozen" in place during the interaction. (For a recent review of this approach see Ref. 14.) Clearly, given a suitable nucleon-nucleon force and the appropriate wave functions, any spin-dependent observable can be calculated using the resulting folded potential. (In some cases it is important to consider exchange effects as well, but this is clearly also possible in principle.) That this approach is by itself inadequate is made apparent by the general failure of folding model calculations to account for a wide variety of experimentally observed spin-dependent phenomena, ranging from vector analyzing powers in ^{6}Li and ^{7}Li scattering[1] to spin-flip measurements in several different systems.[2,5] Basically, the spin dependence in the composite system, which in the folding model arises from spin-orbit and tensor components in the nucleon-nucleon interaction, is diluted by the pairing of the nucleon spins in the target and projectile ground states. Quantitatively, the effects predicted for projectiles with masses between 6 and 13 by this model are between one and two orders of magnitude smaller than those observed.

Essentially all of the attempts to account for the large effects observed experimentally involve spin dependence which arises through higher order (coupled channels) effects in the reaction mechanism. Recently, for example, Nishioka *et al.* explained the sign and magnitude of the effective spin-orbit potential in the ^{6,7}Li interaction with ^{58}Ni by including the strong coupling of excited states of the projectile to the elastic channel.[12] Also, Liu *et al.*[15] have performed detailed coupled channels calculations of the measured spin-flip probability in the $^{13}C+^{24}Mg$ system, including both inelastic scattering and single nucleon transfer channels as intermediate states. Reasonable agreement with the existing (very sparse) experimental data was obtained without the necessity for introducing any phenomenological $\mathbf{l}\cdot\mathbf{s}$ term in the optical potentials. Finally, Imanishi and von Oertzen[16] have recently published a coupled-reaction-channels analysis of elastic and inelastic scattering in the $^{12}C+^{13}C$ system, where spin-flip measurements have also been reported experimentally. At low energies (much lower than those at which experimental data exist), they were able to show that a spin-dependent interaction of approximately the $\mathbf{l}\cdot\mathbf{s}$ type arises naturally from a consideration of coupled channels effects in both inelastic scattering and transfer channels.

The present work was undertaken as part of a program

 ©1985 The American Physical Society

investigating the general question of spin dependence in scattering processes involving light nuclei. The particular question we wished to investigate was whether we could find a system in which a small number of calculable processes provide the main contribution to the spin-dependent observables, and to design an experiment to distinguish among them. The reaction we have investigated is

$$^{12}C + {}^{13}C \rightarrow {}^{12}C^* + {}^{13}C\,, \tag{1}$$

where $^{12}C^*$ refers to the first excited state of ^{12}C at $E_x = 4.43$ MeV. In lowest order this reaction can be considered to proceed via the two diagrams illustrated in Fig. 1. Figure 1(a) shows non-exchange inelastic scattering; the ^{13}C is preferentially emitted in the forward direction; Fig. 1(b) illustrates neutron transfer. In this case the $^{12}C^*$ comes off preferentially in the forward direction.

The central question motivating our investigation is whether spin-dependent observables can be accounted for without the necessity of introducing a phenomenological spin-orbit force directly into the optical potential describing the relative motion of ^{12}C and ^{13}C. Observables will be assumed to acquire spin dependence only through the angular momentum quantum numbers describing the bound states involved in the stripping diagram (b). It might seem at first that this is simply another manifestation of a spin-dependent nucleon-nucleon force, in the sense that, say, the $p_{1/2}$ and $p_{3/2}$ energy levels of ^{13}C have different binding energies. That this is not the case can easily be seen by considering the analogous situation in atoms, where the (relativistic) spin-orbit effect is very small and most of the difference between (say) the energies of the singlet and triplet states of the helium atom arises because of the difference in electrostatic repulsion required by the Pauli principle. Thus, if only central forces acted between nucleons, processes such as (b) above would give rise to spin-dependent effects. The case considered in the present work is a particularly advantageous one to search for such effects, since observations can be made in kinematic regions where processes (a) and (b) are separately dominant; the question then becomes whether a consistent analysis of all the data is possible without the need to introduce an explicitly spin-dependent force.

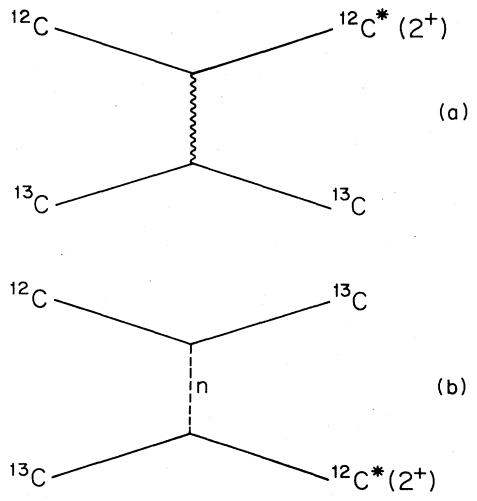

FIG. 1. Diagrams illustrating the dominant lowest order reaction mechanisms in the $^{12}C + {}^{13}C$ system: (a) inelastic scattering; (b) single neutron transfer.

Reaction (1) has been studied experimentally by Tanaka *et al.*, at a bombarding energy of 87 MeV.[5] Spin-dependent effects were isolated using particle-γ coincidence studies with γ rays emitted perpendicular to the reaction plane. The results of Ref. 5 were interpreted by introducing a phenomenological spin-orbit potential of the $\mathbf{l}\cdot\mathbf{s}$ type into diagram (a) above. Diagram (b) was completely neglected; the justification cited was a theoretical calculation using the distorted-wave Born approximation (DWBA) which suggested that process (b) was negligible under the experimental conditions used.

In the present study we have attempted to isolate the effects of the two processes (a) and (b) and interference between them in as model-independent a way as possible. Particle-γ angular correlation measurements were used to infer the magnetic substate populations of the 2^+ state in ^{12}C for events in which the ^{13}C is emitted in either the forward or backward directions. As will be shown, these measurements place important constraints on the interpretation of the reaction mechanism in terms of processes (a) and (b).

The remainder of this paper is organized as follows. Section II gives some theoretical background concerning spin-dependent interactions in nucleus-nucleus scattering and the use of angular correlation measurements to study them. Section III describes the experimental measurements. The results are presented in Section IV, and are interpreted in terms of theoretical calculations of processes (a) and (b). Finally, our conclusions are presented in Section V, with particular attention being paid to the question of model dependence of the results.

II. ANGULAR CORRELATION METHOD

In any two body reaction [we use the notation A(a,b)B], the transition amplitude between definite magnetic substates, $T_{m_a M_A m_b M_B}(\hat{\mathbf{k}}_b)$, contains all possible information concerning the dynamics of the reaction. In cases where interest is focussed on terms in the interaction involving the intrinsic angular momenta of the projectile or ejectile (s_a or s_b), measurements of observables involving magnetic substates directly are of particular importance. Examples include the use of polarized beams and/or targets (selection of M_A or m_a), as well as observation of the spin orientation of the reaction products b or B, either by double scattering or by coincident observation of subsequent decay radiation. In the present work we use the well-known technique of particle-γ angular correlations to study moments of the density matrix of the final 2^+ state B^* in reaction (1). The method has been extensively described in the literature[17] so only a brief summary will be given here. We use a coordinate system with the $\hat{z}$ axis along $\mathbf{k}_a \times \mathbf{k}_b$ and the $\hat{x}$ axis along $\mathbf{k}_a$. Measurements are made of the normalized particle-γ angular correlation function $W(\theta_\gamma, \phi_\gamma)$, where

$$\frac{d^2\sigma}{d\Omega_b d\Omega_\gamma} = \frac{1}{4\pi}\left[\frac{\Gamma^B_{\gamma c}}{\Gamma^B}\right] W(\theta_\gamma,\phi_\gamma)\frac{d\sigma}{d\Omega_b} , \quad (2)$$

with $d^2\sigma/d\Omega_b d\Omega_\gamma$ and $d\sigma/d\Omega_b$ being, respectively, the double and single differential cross sections for detecting a particle in the direction specified by Ω_b and a γ ray in the direction specified by Ω_γ. The branching ratio, $\Gamma^B_{\gamma c}/\Gamma^B$, is the probability that the state B, once formed, emits the γ ray labeled c. With this normalization, $W = 1$ for a transition in which the γ ray is emitted isotropically. The function W is determined completely by the normalized density matrix $\rho_{M_B M'_B}(\hat{\mathbf{k}}_b)$. The diagonal elements $\rho_{M_B M_B}$ give the probability of the M_Bth substate being populated, whereas the off-diagonal elements result from interference between the different substates. Any model calculation of the reaction amplitudes $X_{m_a M_A m_b M_B}(\hat{\mathbf{k}}_b)$ determines the density matrix and thus predicts the particle-γ angular correlation. These predictions may then be compared with experiment. Alternatively, it is sometimes possible to determine some or all of the density matrix elements directly from the data in an essentially model-independent fashion. These can then of course be compared with the model predictions. It is this second approach which has been adopted here. Choosing to compare theoretical and experimental density matrix elements directly is most advantageous in cases where the theory predicts some elements very well and others rather poorly. (For example, magnitudes might be well accounted for and phases not, etc.) In such cases information is clearly lost by comparing the predicted and observed angular correlations themselves, since such a comparison in general reflects only the (relatively poor) overall fit.

In general, the normalized ($\mathrm{tr}\rho = 1$) density matrix for a $J_B = 2$ final state requires 12 real numbers to be specified completely. Measurement of the complete particle-γ directional angular correlation over a sphere can determine 8 of these, as follows:

$$\begin{aligned} W(\theta,\phi) = {} & \rho_{00}F^2_{00}(\theta) + (\rho_{22}+\rho_{-2-2})F^2_{22}(\theta) \\ & - (\rho_{11}+\rho_{-1-1})F^2_{11}(\theta) \\ & - 2b_{1-1}\cos(2\phi+\delta_{1-1})F^2_{1-1}(\theta) \\ & + 2b_{2-2}\cos(4\phi+\delta_{2-2})F^2_{2-2}(\theta) \\ & + 2b'_{20}\cos(2\phi+\delta'_{20})F^2_{20}(\theta) , \end{aligned} \quad (3)$$

where the $F^J_{ij}(\theta_\gamma)$ are simple linear combinations of Legendre polynomials and finite geometry attenuation coefficients. [In what follows, the (real) diagonal elements $\rho_{ii}+\rho_{-i-i}$ are abbreviated as m_i.] The notation $\rho_{MM'} = b_{MM'}\, e^{i\delta_{MM'}}$ has been used to designate the magnitude and phase of the off-diagonal elements; b'_{20}, δ'_{20} are defined by

$$b'_{20} = [(b_{20})^2 + (b_{0-2})^2 + 2b_{20}b_{0-2}\cos(\delta_{20}-\delta_{0-2})]^{1/2} , \quad (4a)$$

$$\delta'_{20} = \tan^{-1}\left[\frac{b_{20}\sin(\delta_{20})+b_{0-2}\sin(\delta_{0-2})}{b_{20}\cos(\delta_{20})+b_{0-2}\cos(\delta_{0-2})}\right] . \quad (4b)$$

This is the particular linear combination of $\rho_{M_B M'_B}$ which can be determined from directional correlation measurements alone. Determination of the remaining elements of ρ requires γ-ray polarization measurements.

It is of interest to contrast Eq. (3) with the well-studied case of non-exchange inelastic scattering of spinless particles from a target of zero spin, the best known example being the scattering of α particles. In that case the angular correlation is determined by 5 real numbers, which can be taken as the amplitudes for the $M_B = -2$, 0, and $+2$ substates and two relative phases. It is well known[18] that in this case these amplitudes and phases can be extracted directly from the data; our purpose here is to extend this model-independent treatment to the more complicated general case.

We focus on two specific features of $\rho_{M_B M'_B}$, which are in fact related (see below). First is the well known fact that for inelastic scattering to a final state with even spin and no overall parity change any element of ρ involving $M_B = \pm 1$ vanishes in the absence of spin-dependent forces. The second feature is relevant when particle transfer is the dominant mechanism. If the total transferred angular momentum j is less than the spin of the final state J_B, $\rho_{J_B-J_B}$ vanishes identically. This occurs because the transition amplitude is proportional to a Clebsch-Gordan coefficient $\langle J_A M_A jm \,|\, J_B M_B\rangle$ which ensures that the $J_B = \pm M_B$ substates are only connected to *different* values of M_A. Because different values of M_A contribute incoherently to the final state density matrix, the interference terms vanish.

In the case of interest, for single neutron transfer we have a pickup reaction with $J_A = 1/2$, $s_a = 0$, $s_b = 1/2$, and $J_B = 2$. Assuming the transferred neutron is picked up from the $p_{3/2}$ orbital (the $f_{5/2}$ orbital has negligible occupation probability in the ^{13}C ground state), we have $j = 3/2$ and $\rho_{2,-2} = 0$. The presence or absence of this interference term in the experimental angular correlation can thus be used to test the hypothesis that the reaction mechanism is dominated by transfer; the admixture of a small inelastic scattering amplitude can, for example, lead to detectable interference between the $M_B = \pm 2$ magnetic substates. Because the same optical potentials are involved for both diagrams in Fig. 1, the admixture of inelastic scattering in the kinematic region dominated by particle transfer is related to the presence of significant transfer amplitude at forward angles where inelastic scattering is dominant. Loosely speaking, both are determined by how fast the reaction amplitude falls off with angle. We can thus use all the information available from the angular correlation measurements to attempt to synthesize a complete description of both processes.

III. EXPERIMENTAL PROCEDURE

The experimental arrangement utilized in these measurements is illustrated schematically in Fig. 2. Beams of ^{13}C ions were obtained from the University of Pennsylvania tandem Van de Graaff accelerator. Most of the work reported herein was done using a bombarding energy of 36 MeV, corresponding to $E_{\mathrm{c.m.}} = 17.28$ MeV. Some

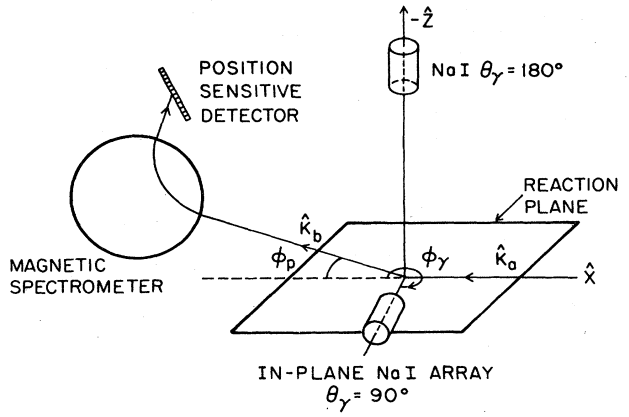

FIG. 2. Schematic diagram of the experimental arrangement used for the particle-γ angular correlation measurements.

measurements were taken at the higher energy of 56 MeV ($E_{c.m.}=26.88$ MeV). Targets consisted of isotopically enriched self-supporting foils of ^{12}C of nominal thickness 100 $\mu g/cm^2$. Reaction products were detected at a laboratory angle of 7° (9° at the higher bombarding energy) using a position-sensitive silicon surface barrier detector (PSD) located in the focal plane of a Browne-Buechner magnetic spectrograph. For the coincidence measurements, the angular acceptance in the center-of-mass system was restricted to $\pm 1.5°$ by the entrance slits to the spectrograph. These same slits defined the reaction plane to within $\pm 1°$. Because of the requirement that the reaction plane be accurately defined, the quadrupole lens[19] which is normally used to enhance the spectrometer solid angle was not used. The simultaneous measurement of the momentum and total energy of the carbon ions accepted by the spectrograph provided isotopic identification of the reaction products. The overall energy resolution was typically 100 keV, except in cases where particles were detected following the prompt γ decay of an excited state, in which case the linewidth is increased by Doppler broadening. (The effect of Doppler broadening increases with the velocity of the ions; for this reason the results at the higher bombarding energy were not as useful as those obtained at 36 MeV; see below.) A typical particle singles spectrum is displayed in Fig. 3.

A similar arrangement was also used to measure a (partial) angular distribution of the ^{12}C and ^{13}C reaction products for both the inelastic and elastic channels. The angular acceptance of the spectrometer was reduced to $\pm 0.15°$ for these measurements, which were normalized using a monitor detector fixed at a laboratory scattering angle of 30°. Spectra were recorded at intervals of 1° between laboratory angles of 6° and 20°. The absolute cross section was obtained by normalizing the measured elastic scattering to that given by Westfall *et al.*[20]

Returning to the coincidence measurements, coincident γ rays were detected by an array of 7.62 cm $\times$10.16 cm NaI(Tl) scintillation counters. For the 36 MeV measurements three of these were located in the reaction plane ($\theta_\gamma=90°$), while the fourth was located along the $\hat{z}$ axis, i.e., in the direction perpendicular to the reaction plane.

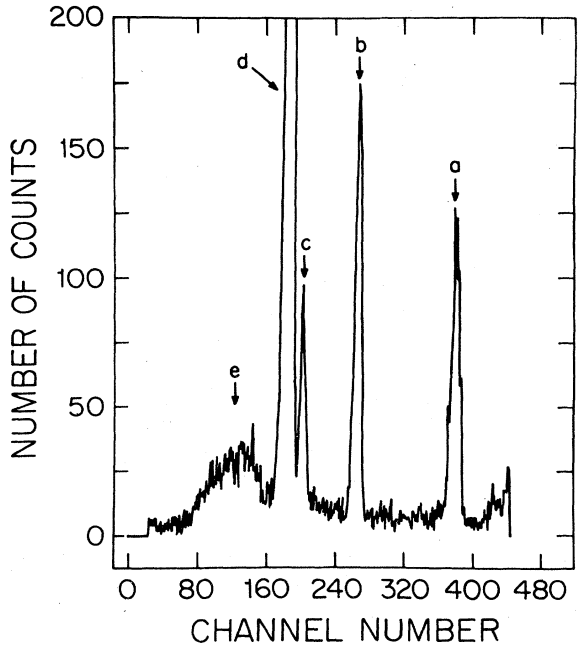

FIG. 3. Singles spectrum of particles detected in the magnetic spectrograph at a laboratory angle of 7°, $E_{c.m.}=17.28$ MeV. The groups are labelled as follows: a, ^{12}C excited, $E_x=4.43$ MeV 2^+ state, ^{13}C detected; b–d, ^{13}C excited, $E_x=3.09$, 3.68, 3.85 MeV, respectively, ^{12}C detected; e, ^{12}C excited, $E_x=4.43$ MeV, ^{12}C detected. Note the Doppler broadening of group e, in which the ^{12}C nucleus is detected after its γ decay in flight.

The detectors were placed 20 cm from the target, and were shielded by 0.64 cm of Pb absorber to harden the γ spectrum, thereby permitting an increase in the usable beam current on target. For the 56 MeV measurements, five NaI(Tl) counters were used. Two were placed in the reaction plane, two at $\theta_\gamma=135°$, and one along the $\hat{z}$ axis at $\theta_\gamma=180°$. In both cases the detectors at θ_γ angles different from 180° could be rotated about the target, so several points could be measured during the course of a run. Singles rates in the γ detectors were kept at or below 50 000 Hz. For the crucial detector located perpendicular to the reaction plane, coincidence losses were monitored by generating artificial coincidences using a pair of pulsers operated in time coincidence. One of these was fed into the energy signal of the PSD; the other provided a current pulse to a light-emitting diode viewed by the photomultiplier of the γ detector at $\theta_\gamma=180°$. In the data reduction procedure these artificial coincidences were processed in the same way as genuine events. Comparing the "singles" and "coincidence" events for the pulsers gives a direct measure of the fraction of events in which a coincidence is lost, for example through pulse pile-up in the γ detector. The losses corrected in this way were as high as 25% for the runs at $E_{^{13}C}=36$ MeV, and about 15% at the higher bombarding energy. Because the pulser was not triggered at a rate proportional to the beam, the pulser events were weighted by the coincidence rate in the data replay procedure.

The signals from the detectors were processed by a standard fast-slow coincidence system. The data were

event-recorded onto magnetic tape for subsequent off-line analysis. The data reduction procedure consisted of replaying the event tapes and generating γ spectra for the various detectors in coincidence with different particle groups as detected in the spectrograph (e.g., $^{12}C^*$, ^{13}C, etc.). Corrections were applied for coincidence losses, γ-ray absorption in the scattering chamber walls and Pb absorbers, accidental coincidences, and the relativistic transformation of detector solid angles as required by the decay in flight of the excited ^{12}C nuclei.

Determination of the number of counts in each spectrum is complicated by the (slightly) different line shapes in the NaI(Tl) detectors and by poor statistics in some spectra. The procedure used consisted of integrating the region of the spectrum corresponding to the full-energy, first- and second-escape peaks. Monte Carlo calculations[21] of the detector response showed satisfactory agreement with the experimentally observed spectra in this energy region. In addition to counting statistics, an estimate of the uncertainty of choosing the region of integration has been included in the experimental error. The Monte Carlo calculations were also used to calculate the absolute efficiency of the γ detectors. This is most important in the case where the angular correlation is only measured in the reaction plane and perpendicular to it. Knowledge of the angular correlation integrated over 4π (obtained from the measured number of singles in the particle detector and the calculated efficiency of the γ detectors) is then extremely useful in constraining the fits (see below).

The data reduction procedure, including the absolute efficiency determination, was checked by using the reaction $^{13}C(^{12}C,^{12}C)^{13}C^*(E_x=3.09$ MeV). (These data were accumulated simultaneously with the angular correlation measurements for the $E_x=4.43$ MeV 2^+ state.) Because the total angular momentum of the $E_x=3.09$ MeV level is 1/2, the angular correlation must be isotropic in the rest frame of the recoiling nucleus. The measured angular correlation for this state is shown in Fig. 4. The experimental angular correlation is in fact found to be isotropic within the estimated experimental errors. Moreover, the absolute number of counts is in agreement with the predictions of the Monte Carlo calculations described above.

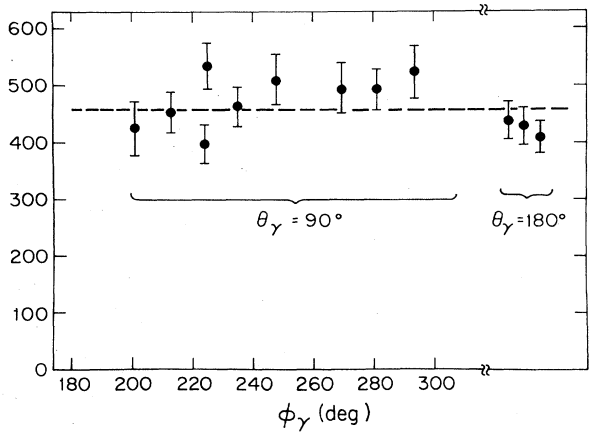

FIG. 4. Experimentally observed angular correlation for inelastic scattering to the $J^\pi=(1/2)^+$ first excited state of ^{13}C. The solid line shows the predicted angular correlation using the calculated efficiency of the γ-ray detectors. This angular correlation was accumulated simultaneously with the experimental spin-flip data (see the text).

The next phase of the data reduction consists of determining the density matrix elements $\rho_{M_B M_B'}$ from a least squares fit to the measured angular correlation. A grid search algorithm described by Bevington[22] was used, in which the fitting parameters were varied sequentially, iterating until a stable minimum in χ^2 in the multiparameter space was found. The procedure was tested using artificially generated data with realistic "scatter" in order to ensure that convergence to the correct solution was achieved in situations similar to those found in the actual experimental data. Inspection of Eq. (3) shows that a measurement of the angular correlation over a full sphere can in principle determine eight independent parameters: two of the three diagonal elements m_0 (ρ_{00}), m_1 ($\rho_{11}+\rho_{-1-1}$), m_2 ($\rho_{22}+\rho_{-2-2}$), and the interference terms $b_{1,-1}$, $\delta_{1,-1}$, $b_{2,-2}$, $\delta_{2,-2}$, b'_{20} and δ'_{20}. Additional restrictions occur as a result of the finite range of data in the present experiment. In the actual fits the sum of the diagonal elements was constrained by the known integrated angular correlation obtained from the particle singles. Because γ rays were measured only at $\theta_\gamma=180°$ and 90° there is a problem in determining the interference terms involving the $M_B=0$ and $|M_B|=2$ magnetic substates. (The angular correlation in the case where only $\rho_{00}\neq 0$ peaks at $\theta_\gamma=45°$ and vanishes at $\theta_\gamma=180°$ and 90°.) This implies that the in-plane angular correlation is insensitive to b'_{20} and δ'_{20}. To test whether our ignorance of these terms affects other aspects of the fitting procedure, fits were made in which interference terms between the $M_B=0$ and $|M_B|=2$ substates were both included and omitted. As expected, these fits resulted in large uncertainties in b'_{20}, δ'_{20}. (A very small dependence on these parameters does exist owing to the finite size of the γ ray detectors.) More important, however, is the fact that the other parameters of the fits were not affected to any significant extent.

IV. RESULTS

A. Model independent analysis

1. Forward angle data

The density matrix elements obtained at $E_{\text{c.m.}}=17.28$ MeV from the fit at $\phi_b(\text{c.m.})=15.8°$ are shown as Fit 1 in Table I. b'_{20}, δ'_{20} have been omitted from this fit, but including them (Fit 2) produces essentially identical results. A small spin-flip signal (i.e., m_1 not equal to zero) is clearly observed. Because the spin flip is small, it is not possible to determine the interference between the $M_B=\pm 1$ substates. The calculated angular correlation is compared to the data in Fig. 5; in the reaction plane the $\cos 4\phi$ pattern characteristic of interference between the $M_B=\pm 2$ amplitudes is clearly dominant. Similar results were obtained at $E_{\text{c.m.}}=26.88$ MeV, $\phi_b(\text{c.m.})=19.7°$. (See Fit 3 of Table I.) The spin flip is somewhat smaller, but the other density matrix elements are nearly identical to those obtained at the lower energy. The measured angular

TABLE I. Fits for $^{12}C + ^{13}C$ at ϕ_b(c.m.)=15.8° ($E_{c.m.}$=17.28 MeV), ϕ_b(c.m.)=19.7° ($E_{c.m.}$=26.88 MeV).

	$E_{c.m.}$=17.28 MeV		$E_{c.m.}$=26.88 MeV
	Fit 1	Fit 2	Fit 3
m_0	0.35±0.05	0.36±0.05	0.394±0.007
m_1	0.036±0.003	0.036±0.003	0.015±0.004
m_2	0.61±0.03	0.61±0.03	0.592±0.008
b_{2-2}	0.223±0.013	0.232±0.013	0.226±0.005
δ_{2-2}	10.°±2°	10.°±2°	224°±3°
b'_{20}		0.7±0.2	0.578±0.011
δ'_{20}		−32°±32°	−59°±2°
χ^2/ν	1.6	1.5	1.2
ν	6	4	2

correlations are compared to the fits in Fig. 6. Note that in this case b'_{20} and δ'_{20} are well determined as a consequence of having measured the angular correlation at θ_γ=135°. The measured spin-flip probability at $E_{c.m.}$=26.88 MeV is similar to that reported by Tanaka *et al.* (Ref. 5) at $E_{c.m.}$=41.76 MeV, whereas at the lower bombarding energy we find a value approximately twice as large.

2. *Backward angle data*

As noted above, at ϕ_b(c.m.)=164.9° neutron transfer is expected to be the dominant process. Consequently, a first attempt was made to fit the measured angular correlation omitting interference terms between the $M_B=\pm2$ magnetic substates. In this case, the structure of the in-plane angular correlation results primarily from interference between the $M_B=\pm1$ amplitudes. The observed value of m_1 gives an upper limit to the value of this interference term (i.e., when the $M_B=\pm1$ amplitudes are equal); this value is considerably smaller than that required by the data. The results of this fit are shown as the dashed curve in Fig. 7(a) and Fit 1 in Table II. It is worth noting that the point at (θ_γ, ϕ_γ)=(0°,0°) is essential for a meaningful fit. The solid curve in Fig. 7(a) shows the result of a fit in which only the in-plane angular correlation was used, still with $b_{2,-2}=0$. The parameters for this fit are labelled Fit 2 in Table II; they are inconsistent with the correct density matrix. For example, they predict a yield at (θ_γ,ϕ_γ) = (180°,0°) about 2.5 times larger than observed.

The data thus require interference between the $M_B=\pm2$ amplitudes. A fit including this term is shown in Fig. 7(b); the resulting parameters are labelled Fit 3 in Table II. In this case, the difference with and without including b'_{20} are slightly larger than at forward angles, but still comparable to the errors in the fitting procedure. (The fit without including them is shown.)

Two conclusions emerge from these data. First, the spin-flip probability is quite large; this is not unexpected for a transfer reaction. Second, the presence of detectable interference between the $M_B=\pm2$ substates implies that some process other than pure neutron transfer is contributing to the back-angle yield. The most likely candidate for this process is direct inelastic scattering.

The appearance of an inelastic scattering contribution to the back angle yield suggests that the observed spin flip at forward angles may be the result of the small transfer amplitude which survives at forward angles. These two are of course related, since both are suppressed by the same mechanism, namely the forward-peaked diffractive nature of direct reaction amplitudes. The idea that both observations have a common origin motivated the reaction model calculations described in the following subsection.

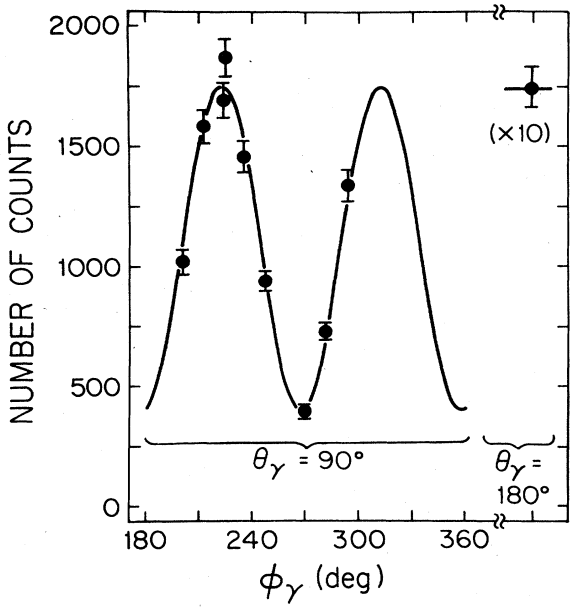

FIG. 5. Particle-γ angular correlation measured at ϕ_b(c.m.)=15.8°, $E_{c.m.}$=17.28 MeV. The solid curve is calculated using the parameters of Fit 1 in Table I. Note that the point at θ_γ,ϕ_γ=(180°, 0°) is plotted at 10 times its actual value.

B. Comparison with reaction model calculations

1. *Spin-orbit component in the optical potential*

If the present experimental results at forward angles are interpreted by adding a spin-orbit term

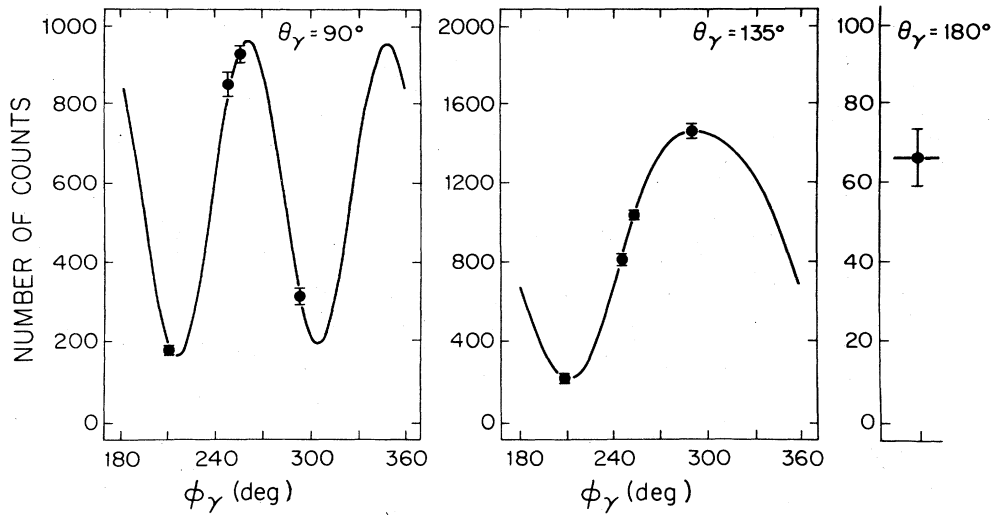

FIG. 6. Particle-γ angular correlation observed at ϕ_b(c.m.)=19.7°, $E_{\text{c.m.}}$=26.88 MeV. Note the different periodicity for the ϕ dependence of the angular correlation at the different values of θ_γ.

$$V_{ls}(r) = -\left[\frac{\hbar}{m_\pi c}\right]^2 \frac{V_{so}}{r}\frac{d}{dr}\left[1+\exp\left(\frac{r-R_{so}}{a_{so}}\right)\right]^{-1} \mathbf{l}\cdot\boldsymbol{\sigma} \tag{5}$$

to the ^{12}C - ^{13}C optical potential, then the value of V_{so} required to fit the present data is 3.5 MeV at $E_{\text{c.m.}}=17.28$ MeV and 6 MeV at $E_{\text{c.m.}}=26.88$ MeV. The spin-orbit strength obtained here is comparable to that reported in Ref. 5, although a quantitative comparison is made difficult by the fact that experiments at different bombarding energies are being compared. In addition, we were unable to reproduce the detailed results of the DWBA calculations reported in Ref. 5. With the same optical potentials, we find a spin-flip probability only about half as large, and a somewhat different angular distribution for the scattered particles as well. Despite these uncertainties, it appears safe to conclude that if the observed spin-flip probability is to be explained by a spin-orbit potential of the form (5), the value of V_{so} required by the present work and that of Ref. 5 is between 1.5 and 6 MeV for center-of-mass energies between about 15 and 40 MeV.

2. Prediction using transfer

We next investigate whether the present data can be accounted for by assuming that the optical potential between ^{12}C and ^{13}C is not explicitly spin dependent. For simplicity, a purely central interaction is assumed. The nonvanishing value of ρ_{11} in this case comes only from the single neutron transfer diagram [Fig. 1(b)].

In order to test this hypothesis, the two contributions in Fig. 1 have been calculated using the distorted-wave Born approximation (DWBA). The inelastic scattering was calculated using the zero-range DWBA code DWUCK4[23] and was normalized to the experimental angular distribution at forward angles. The single neutron transfer contribution was calculated with the full finite-range DWBA code DWUCK5.[23] The transfer amplitude should be evaluated at $(\pi-\theta_b,\phi_b=\pi)$. Since the DWBA code calculates amplitudes for $\phi_b=0°$, a rotation by π about the $\hat{z}$ axis is required. In addition, because of the structure of the pro-

TABLE II. Fits for ^{12}C + ^{13}C at ϕ_b(c.m.) =164.9°.

	Fit 1	Fit 2	Fit 3
m_0	0.20±0.05	0.30±0.05	0.08±0.05
m_1	0.23±0.02	0.58±0.03	0.226±0.013
b_{1-1}	0.114±0.014	0.24±0.02	0.113±0.008
δ_{1-1}	−2.9°±0.5°	17°±2°	−17°±5°
m_2	0.57±0.03	0.127±0.006	0.69±0.04
b_{2-2}			0.108±0.012
δ_{2-2}			−102°±5°
χ^2/ν	9.8	1.3	1.2
ν	6	7	4

gram DWUCK5, the transfer contribution had to be calculated as the pickup reaction $^{13}C(^{12}C,^{13}C)^{12}C^*$. The inelastic scattering reaction was calculated by DWUCK4 as $^{12}C(^{13}C,^{13}C)^{12}C^*$. Thus, the transfer amplitude must be subjected to an additional rotation by π about the axis perpendicular to the reaction plane before it is added to the inelastic amplitude.

The amplitudes were combined according to the above prescriptions to yield

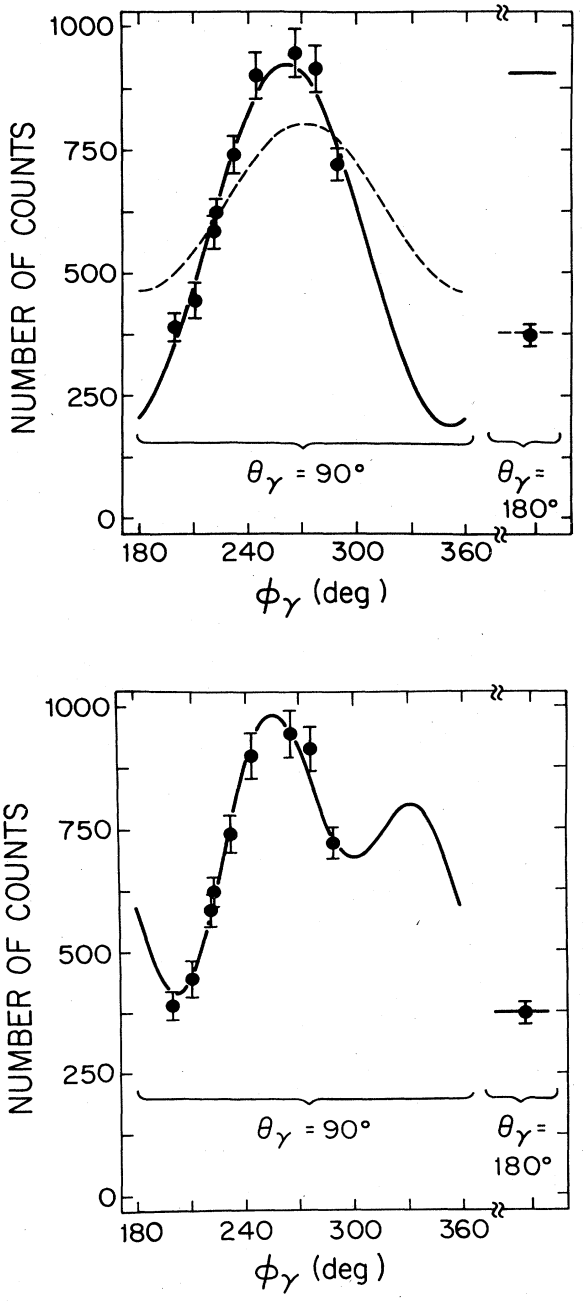

FIG. 7. (a) Particle-γ angular correlation for ϕ_b(c.m.)=164.9°, $E_{c.m.}$=17.28 MeV. The dashed and solid curves correspond to Fits 1 and 2 of Table II, respectively (see text). (b) Same data as (a). The solid curve corresponds to Fit 3 in Table II, and includes interference between the $M_B=\pm 2$ substates.

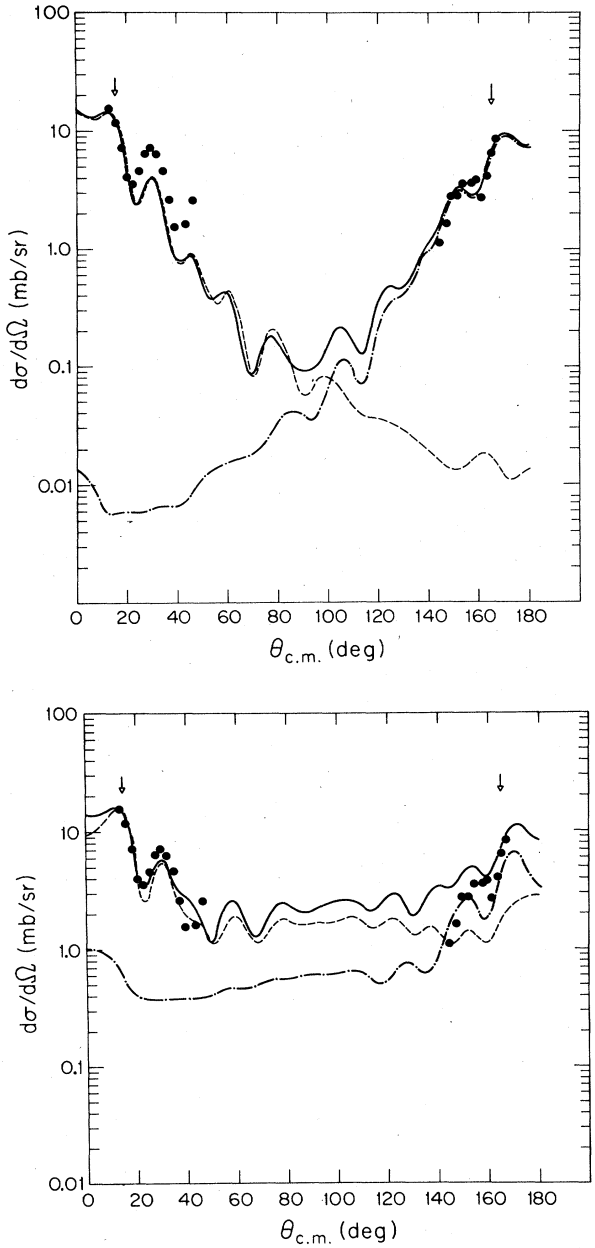

FIG. 8. (a) Partial singles angular distribution for the inelastic scattering of ^{13}C from a ^{12}C target, leaving the target in its first excited 2^+ state. The curves are DWBA calculations using the original optical potential of Table IV. The dashed curve is the inelastic scattering cross section, while the dash-dot curve shows the contribution of single nucleon transfer. The solid curve is the coherent sum of the two, as discussed in the text. The vertical arrows show the angles where particle-γ angular correlations were measured. (b) Same as (a) except that the curves correspond to the modified optical potential of Table IV.

TABLE III. Comparison of density matrix elements extracted from the data with those predicted by DWBA calculations using original and modified optical potentials (see text).

Parameter	15.8°			164.9°		
	Expt.	Original	Modified	Expt.	Original	Modified
m_0	0.35 ±0.05	0.24	0.22	0.08±0.05	0.10	0.25
m_1	0.036±0.003	0.0	0.022	0.23±0.01	0.30	0.19
m_2	0.61 ±0.03	0.76	0.76	0.69±0.04	0.60	0.56
b_{1-1}	0.0	0.0	0.0	0.11±0.01	0.16	0.06
b_{2-2}	0.22 ±0.01	0.35	0.34	0.11±0.01	0.01	0.12

$$T^{\text{total}}_{m_a M_A m_b M_B}(\theta_b) = T^{\text{inel}}_{m_a M_A m_b M_B}(\theta_b) + (-)^{A+J_B+s_b-J_A-s_a} T^{\text{trans}}_{-m'_a-M'_A-m_b-M_B}(\pi-\theta_b)\,\delta_{m'_a,M_A}\delta_{M'_A,m_a}.$$

All amplitudes are evaluated at $\phi_b = 0°$. A is the mass of the exchanged core. The last two Kronecker δ factors occur because of the interchange of the target and projectile in the transfer calculation, as noted above. The same optical potential was used for both the inelastic scattering and transfer calculations. The strength of the transfer amplitude was adjusted to fit the back-angle yield. The combined amplitudes were integrated over the finite angular acceptance of the particle detector to facilitate a direct comparison with the experimentally determined $\rho_{M_B M'_B}$. The comparison at $E_{\text{c.m.}} = 17.28$ MeV using an optical potential taken from the literature[20] is shown in the columns labelled "original" in Table III.

Two points emerge from this comparison. The predicted spin-flip probability at forward angles is negligible, as is the interference between the $M_B = \pm 2$ substates at backward angles. This merely reflects the strongly forward (backward) peaked nature of the inelastic scattering (transfer) amplitudes. In an attempt to improve the agreement between theory and experiment we have (in a purely phenomenological way) adjusted the imaginary part of the optical potential in order to reduce the strong attenuation of both amplitudes with increasing scattering angle. The resulting potential is given in row 2 of Table IV, and the resultant density matrix is shown in the "modified" columns of Table III. The predicted spin-flip probability is now within a factor of 2 of that observed. Moreover, the predicted interference between the $M_B = \pm 2$ substates is reproduced very well. The consistency between these two effects strongly supports the hypothesis of a common origin. The modified optical potential also fits the measured particle angular distribution somewhat better at forward angles, although the fit at backward angles is somewhat worse. The measured partial singles angular distributions are shown in Figs. 8(a) and 8(b), along with the predictions of calculations using the original and modified optical potentials, respectively. The inelastic scattering and transfer cross sections are shown separately, along with their coherent sum, to illustrate the interplay of the two amplitudes as discussed above.

It is important to recognize the crude nature of the present treatment. Note, for example, that the remaining density matrix elements are fitted rather poorly by the modified potential. These calculations are intended to be understood only as a schematic attempt to demonstrate the plausibility of the assertion that the nonvanishing ρ_{11} observed at forward angles results from the effects of single nucleon transfer.

V. CONCLUSIONS

The principal model-independent conclusion which can be drawn from the present work is that a clear spin-flip signal is observed at forward angles in the $^{12}C + {}^{13}C$ system at energies of 17.28 and 26.88 MeV in the center-of-mass system. In addition, it is found that the data in the kinematic region where single neutron transfer is expected to be dominant require the presence of some other reaction mechanism, most likely inelastic scattering. Taken together, these results suggest that the observed spin flip can be explained by a small transfer amplitude at forward angles, and do not require the presence of an explicitly spin-dependent component in the nucleus-nucleus optical potential. This is consistent with the result that spin-orbit forces derived from the folding model are far too small to explain the observed effects. It is also consistent with results in other systems, in which the observed spin-flip effects have mainly been attributed to higher order effects involving either inelastic scattering or sequential transfer.

TABLE IV. Optical model potentials used for $^{13}C + {}^{12}C$ reactions.

	V_R (MeV)	r_R (fm)	a_R (fm)	W_v (MeV)	r_I (fm)	a_I (fm)	r_c (fm)
Original	86.602	1.084	0.586	9.563	1.263	0.329	1.084
Modified	86.602	1.084	0.586	16.19	0.62	0.329	1.084

It thus appears that the spin dependence which is observed in nucleus-nucleus reactions at moderate energies is generally a fairly complicated result of the contributions of higher order many-body processes, and is unlikely to illuminate the description of such scattering processes in terms of a simple static two-body potential.

This work was supported by the National Science Foundation.

---

*Present address: Polaroid Corporation, Cambridge, MA.
†Present address: Department of Physics, University of Arizona, Tucson, AZ.

[1]W. Weiss, P. Egelhof, K. D. Hildebrand, D. Kassen, M. Makowska-Rzeszutka, D. Fick, H. Ebinhaus, E. Steffans, A. Amakawa, and K.-I. Kubo, Phys. Lett. **61B**, 237 (1976).
[2]W. Dünnweber, P. D. Bond, C. Chasman, and S. Kubono, Phys. Rev. Lett. **43**, 1642 (1976).
[3]S. Kubono, D. Dehnhard, D. A. Lewis, T. K. Li, J. L. Artz, D. J. Weber, P. Ul Ellis, and A. Dudek-Ellis, Phys. Rev. Lett. **38**, 817 (1977).
[4]P. Wust, W. von Oertzen, H. Ossenbrink, H. Lettau, H. G. Bohlen, W. Saathoff, and C. A. Wiednor, Z. Phys. A **291**, 151 (1979); W. von Oertzen, E. R. Flynn, J. C. Peng, J. W. Sunier, and R. Brown, *ibid.* **301**, 365 (1981); **310**, 275 (1983); W. von Oertzen, H. von Lettau, H. G. Bohlen, and D. Fick, *ibid.* **315**, 81 (1984).
[5]M. Tanaka, J. Kawa, T. Fukuda, T. Shimoda, K. Katori, S. Nakayama, I. Miura, and H. Ogata, Phys. Lett. **106B**, 293 (1981).
[6]F. Petrovich, D. Stanley, L. A. Parks, and P. Nagel, Phys. Rev. C **17**, 1642 (1978).
[7]J. Meyer, R. S. Nahabetian, and E. Elbaz, Nuovo Cimento **22**, 355 (1978).
[8]K. Sugimoto, N. Takahashi, A. Mizobuchi, Y. Nojiri, T. Minamisono, M. Ishihara, K. Tanaka, and H. Kamitsubo, Phys. Rev. Lett. **39**, 323 (1977).
[9]W. Trautmann, C. Lauterbach, J. de Boer, W. Dunnweber, G. Graw, W. Hamann, W. Hering, and H. Puchta, Nucl. Instrum. Methods **184**, 449 (1981).
[10]W. Dünnweber, in *Nuclear Structure and Heavy Ion Dynamics,* edited by L. G. Moretto and R. A. Ricci (North-Holland, Amsterdam, 1984).
[11]P. D. Bond, Z. Phys. A **319**, 57 (1984).
[12]H. Nishioka, R. C. Johnson, and J. A. Tostevin, Phys. Rev. Lett. **48**, 1795 (1982); H. Nishioka, J. A. Tostevin, R. C. Johnson, and K.-I Kubo, Nucl. Phys. **A415**, 230 (1984).
[13]F. H. Schmidt, R. E. Brown, J. B. Gerhart, and W. A. Kolasinski, Nucl. Phys. **52**, 353 (1964).
[14]G. R. Satchler, *Direct Nuclear Reactions* (Oxford University Press, Oxford, 1983).
[15]Q. K. K. Liu, P. J. Ellis, and S. Chakravarti , Phys. Lett. **143B**, 60 (1984).
[16]B. Imanishi and W. von Oertzen, Phys. Lett. **118B**, 273 (1982).
[17]F. Rybicki, T. Tamura and G. R. Satchler, Nucl. Phys. **A146**, 659 (1970); N. S. Zelenskaya and I. B. Teplov, *ibid.* **A406**, 306 (1983).
[18]T. D. Hayward and F. H. Schmidt, Phys. Rev. C **1**, 923 (1970).
[19]H. A. Enge, Rev. Sci. Instrum. **29**, 885 (1958).
[20]G. Westfall and S. A. A. Zaidi, Phys. Rev. C **14**, 619 (1976).
[21]C. D. Zerby and H. S. Moran, Nucl. Instrum. Methods **14**, 115 (1961); computer program MORN, modified by M. J. L. Yates, Nucl. Instrum. Methods **23**, 152 (1963).
[22]P. R. Bevington, *Data Reduction and Error Analysis for the Physical Sciences,* (McGraw-Hill, New York, 1969).
[23]P. D. Kunz, computer codes DWUCK4 and DWUCK5, University of Colorado.